HOKKAIDO UNIVERSITY

Title	A Catalytic Strategy for Selective Production of 5-Formylfuran-2-carboxylic Acid and Furan-2,5-dicarboxylic Acid
Author(s)	Wiesfeld, Jan J.; Asakawa, Miyuki; Aoshima, Takayuki; Fukuoka, Atsushi; Hensen, Emiel J. M.; Nakajima, Kiyotaka
Citation	ChemCatChem, 14(16), e202200191 https://doi.org/10.1002/cctc.202200191
Issue Date	2022-03-28
Doc URL	http://hdl.handle.net/2115/88653
Rights	This is the peer reviewed version of the following article: [J. J. Wiesfeld, M. Asakawa, T. Aoshima, A. Fukuoka, E. J. M. Hensen, K. Nakajima, ChemCatChem 2022, 14, e202200191.], which has been published in final form at [Link to final article using the DOI]. This article may be used for non-commercial purposes in accordance with Wiley Terms and Conditions for Use of Self-Archived Versions. This article may not be enhanced, enriched or otherwise transformed into a derivative work, without express permission from Wiley or by statutory rights under applicable legislation. Copyright notices must not be removed, obscured or modified. The article must be linked to Wiley ' s version of record on Wiley Online Library and any embedding, framing or otherwise making available the article or pages thereof by third parties from platforms, services and websites other than Wiley Online Library must be prohibited.
Type	article (author version)
File Information	Manuscript revised.pdf

Instructions for use

Hokkaido University Collection of Scholarly and Academic Papers : HUSCAP

A Catalytic Strategy for Selective Production of 5-Formylfuran-2-carboxylic Acid and Furan-2,5-dicarboxylic Acid

Jan J. Wiesfeld[a], Miyuki Asakawa[a], Takayuki Aoshima[b], Atsushi Fukuoka[a], Emiel J.M. Hensen[c]*, Kiyotaka Nakajima[a]*

[a] Dr. Ir. Jan J, Wiesfeld, Miyuki Asakawa, Prof. Dr. Atsushi Fukuoka, Prof. Dr. Kiyotaka Nakajima
Institute for Catalysis
Hokkaido University
Kita 21 Nishi 10, Kita-ku, Sapporo, Hokkaido, 001-0021, Japan
E-mail: nakajima@cat.hokudai.ac.jp
[a] Dr. Takayuki Aoshima
Science & Innovation Center
Mitsubishi Chemical Corporation
1000 Kamoshida-cho, Aoba-ku, Yokohama 227-8502, Japan
[c] Prof. Dr. Ir. Emiel J. M. Hensen
Laboratory of Inorganic Materials & Catalysis, Department of Chemical Engineering and Chemistry, Eindhoven University of Technology
Eindhoven University of Technology
PO Box 513, 5600 MB Eindhoven, The Netherlands
Email: e.j.m.hensen@tue.nl

Supporting information for this article is given via a link at the end of the document.

Abstract: A novel catalytic strategy involving protective chemistry is presented for the selective production of 5-formylfuran-2-carboxylic acid (FFCA) and furan-2,5-dicarboxylic acid (FDCA) from concentrated 5-hydroxymethylfurfural (HMF) solutions. By protecting the reactive formyl group of HMF by acetalization with 1,3-propanediol (PDO), degradation and premature oxidation of HMF is suppressed. A hydroxyapatite-supported Au catalyst can selectively oxidize HMF-acetal in a 10 wt% solution to FFCA-acetal in 94% yield in 2 hours at 373 K under 0.5 MPa of O_2. Deprotection of FFCA-acetal by mineral acids affords FFCA in 98% yield and recovers nearly all PDO. FFCA in a 20 wt% solution can be oxidized to FDCA in 95% yield under similar reaction conditions. The presented chemistry contributes to the development of novel manufacturing routes of prospective biobased monomer precursors using protecting agents.

Introduction

Industrial production of chemicals, energy, and fuels from renewable biomass has received considerable attention recently as a way to reduce our dependence on fossil feedstocks in the transition towards a sustainable chemical industry. The current global production of plastics (> 350 megatons per year) primarily depends on monomers obtained from petroleum oil resources.[1] Therefore, there is increasing interest to convert biomass resources into building blocks for essential plastics.[2,3] Biomass-derived furanics such as furfural and 5-hydroxymethylfurfural (HMF) have been at the center of attention, because these compounds can be derived from lignocellulosic feedstocks and converted to a large variety of monomers.[4,5] Examples include 1,6-hexanediol,[6,7] 1,6-hexanediamine,[8] 6-hydroxyhexanoic acid,[9,10] adipic acid,[10] ε-caprolactone,[10] and terephthalic acid,[11] which can all directly be implemented in current polymerization processes. Furthermore, furan-2,5-dicarboxylic acid (FDCA) and its carboxylates, which are obtained by aerobic oxidation of HMF,[12–20] can be combined with alkylene glycols for the production of polyalkylene furanoates, a new family of biomass-based polyesters with excellent gas-barrier properties.[21–28] Polymerization with ethylene glycol produces polyethylene furanoate (PEF), which has been widely recognized as an alternative to polyethylene terephthalate (PET), which is manufactured from fossil-fuel derived terephthalic acid.[29–32] Successful strategies for obtaining high FDCA yields from HMF employ supported noble metal (Pt, Pd, Au, and Ru) catalysts or unsupported metal oxide (MnO_2 and $MnFeO_x$) catalysts. An overview of the most important contributions is given in **Table S1** of the Supporting Information, distinguishing approaches using base additives or basic support materials.[12–20] Despite potential applications of FDCA and its derivatives as building blocks for polymers, large-scale production of these valuable monomers has not yet been realized. An important challenge is that HMF quickly degrades in concentrated reaction mixtures. Industrial application of HMF is therefore limited to dilute solutions because it avoids the formation of by-products that limit the desired product yield. One important exception is the work performed by Motagamwala in which 7.5 wt% of HMF could be oxidized to FDCA in 94% yield over 5% Pt/C without the use of base. However, the downsides of this approach are the use of an organic solvent (γ-valerolactone) and the operation under an excessively high O_2 pressure of 4 MPa.[33] The use of dilute solutions implies high cost associated with solvent recycling and low productivity. The rapid degradation of HMF is due to the presence of a reactive formyl group, which can engage in undesired condensation and polymerization side-reactions into humins.

Aerobic oxidation of HMF at high concentrations (10-20 wt%) has been studied using a ceria-supported gold catalyst at 413 K in alkaline media.[20] The reaction proceeds through the same cascade mechanism as proposed by Corma et al. for the oxidation of diluted HMF (1 wt%) under otherwise comparable conditions (**Scheme 1a**).[19] The reaction starts with the oxidation of the formyl group in HMF, yielding 5-hydroxymethylfuran-2-carboxylic acid (HMFCA). FDCA is then obtained in two consecutive steps. The hydroxyl group in HMFCA is first oxidized to the formyl group into 5-formylfuran-2-carboxylic acid (FFCA), which is then oxidized in the second step to afford

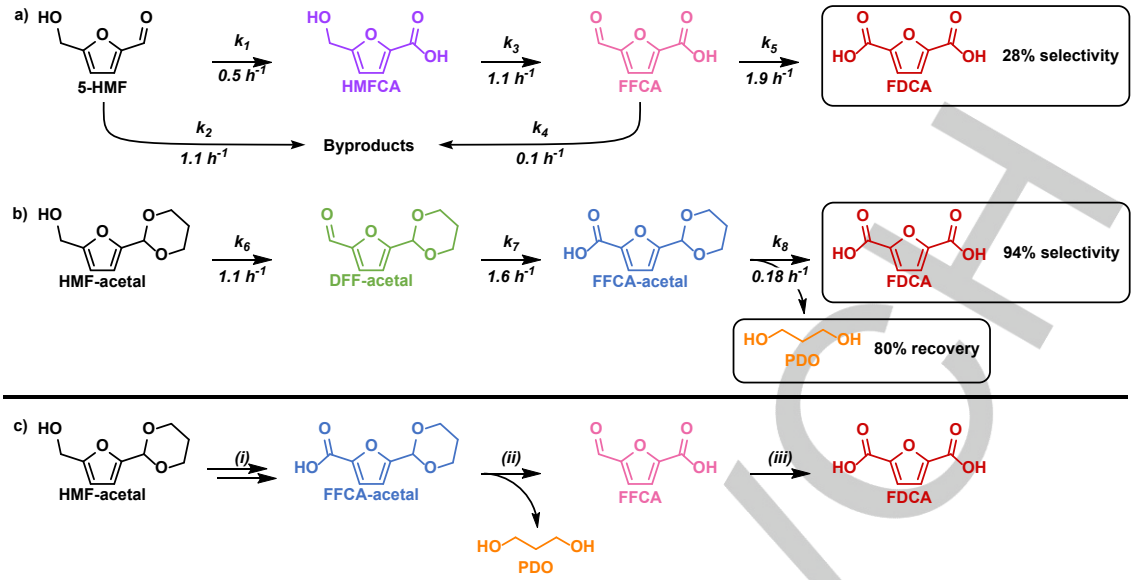

Scheme 1. Reaction pathways describing the direct aerobic oxidation of 5-HMF (a) or HMF-acetal (b) to FDCA. (c) outlines the 3-step approach, in which HMF-acetal is (i) oxidized selectively to FFCA-acetal, (ii) subsequently deprotected to FFCA and separated from PDO, and (iii) finally oxidized to yield FDCA.

FDCA. In a 10 wt% solution, the rate of byproduct formation from HMF is higher (k_2 = 1.1 h^{-1}) than that of HMFCA formation (k_1 = 0.5 h^{-1}). Therefore, byproduct formation is predominant in the first parallel reaction and FDCA was obtained in a limited yield of 28% at complete HMF conversion.

Recognizing the high reactivity, we developed an acetalization strategy to stabilize the formyl group with 1,3-propanediol (PDO) and used the resulting six-membered ring acetal form of HMF(HMF-acetal) in FDCA production. Protective chemistry common in small-scale organic synthesis is currently being explored intensively for biomass conversion.[34–36] HMF-acetal was selectively converted to FDCA in excellent yields (> 90%) even at high concentrations (10-20 wt%) using the same catalyst.[20] The acetal moiety is very stable against deprotection under the applied reaction conditions, *i.e.*, alkaline water. As a result, oxidation is initiated at the hydroxyl group of HMF-acetal, yielding DFF-acetal (monoacetal form of 2,5-diformylfuran) and FFCA-acetal (**Scheme 1b**) consecutively.[20] The final oxidation step to form FDCA occurs at a much slower rate (k_8 = 0.18 h^{-1}) compared to the first (k_6 = 1.1 h^{-1}) and second (k_7 = 1.6 h^{-1}) oxidation steps. This leads to long reaction times to obtain high FDCA yield, having the drawback that PDO liberated under these conditions can be oxidized as well. Consequently, the PDO recovery is limited to approximately 80%. In terms of production volume of end products, such PDO loss is a serious concern for the use of FDCA in polymer manufacture.

To improve the PDO recovery at a high FDCA productivity, we devised a stepwise approach (**Scheme 1c**). The first step entails the selective oxidation of HMF-acetal to FFCA-acetal. In the second step, deprotection of the FFCA-acetal in the reaction mixture recovers free FFCA and PDO. The intermediate FFCA is oxidized to the desired FDCA product in the third step. Adding reaction steps and using protecting group strategies are typically regarded as drawbacks from a green chemistry perspective.[37] However, the approach proposed here enables use of concentrated reactant solutions, which decreases solvent recycle, and the loss of protecting agent PDO can be minimized to a significant extent in the overall process. High recovery of PDO represents a significant advance over the state of the art: in previous work describing the one-pot production of FDCA from the HMF-acetal using Au/CeO_2 catalyst, about 20% of PDO was consumed by oxidative degradation. An additional advantage of this approach is the ability to selectively obtain FFCA. Potential applications of FFCA include its conversion to 5-aminomethylfuran carboxylic acid (AMFCA) through reductive amination, which is a promising monomer for manufacturing biobased polyamide fibers.[38] **Table S1** presents several catalytic systems, which afford FFCA in reasonable yields. However, these approaches cannot halt its subsequent oxidation into FDCA as the formyl group of the intermediate FFCA is easily oxidized to the corresponding carboxylic acid (**Scheme 1a**). In our stepwise reaction system, the formyl group in HMF remains protected during oxidation, which prevents both its degradation and its further oxidation to FDCA.

Kinetic studies supported by computational calculations in our previous work revealed that the final oxidation step in the one-pot oxidation of the HMF-acetal proceeds predominantly through activation of the acetal in FFCA-acetal by Lewis acid sites on the inorganic CeO_2 support (**Scheme S1**).[20] This implies that substituting CeO_2 by a weakly acidic or basic support material will effectively inhibit the final oxidation step and enable the selective production of FFCA-acetal, which is an important step in the proposed approach. To accomplish this, we synthesized gold catalysts supported on amphoteric and basic oxides (CaO, MgO, TiO_2, ZrO_2, Al_2O_3, hydrotalcite (HT), and hydroxyapatite (HAP)), and examined their activity in the aerobic oxidation of HMF-acetal in order to maximize both the FFCA-acetal yield/selectivity and PDO recovery. We also investigated deprotection of the FFCA-acetal to recover free FFCA and PDO. Free FFCA in concentrated (15-25 wt%) solutions was then oxidized to FDCA with the same Au catalyst used in the HMF-acetal oxidation.

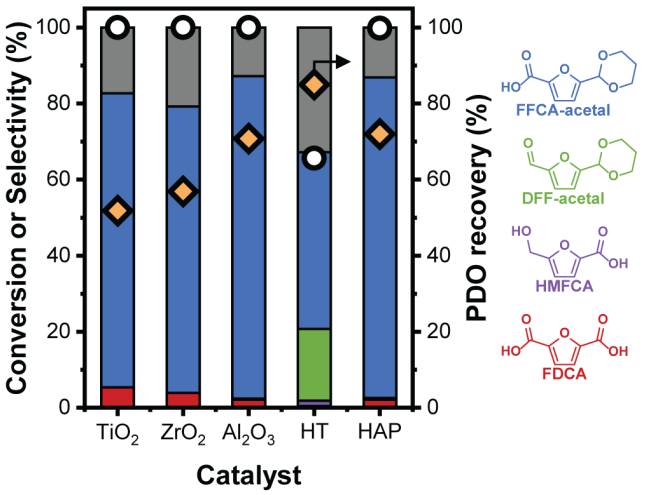

Figure 1. Influence of the support on the gold-catalyzed oxidation of HMF-acetal to FFCA. Blue, green, red, purple, and grey bars show the yield of FFCA-acetal, DFF-acetal, FDCA, HMFCA, and unidentified byproducts, respectively. White circles and orange diamonds represent HMF-acetal conversion and PDO recovery, respectively. Conditions: HMF-acetal, 100 mg; catalyst, 100 mg Au/support; Na_2CO_3, 2 mol. eq. to HMF-acetal; H_2O, 1 mL; O_2, 0.5 MPa; 373 K, 5 h, 750 rpm.

Results and Discussion

Gold was deposited on a series of basic and weakly acidic oxides commonly used as support for catalysts, such as γ-Al_2O_3,[39–41] CaO,[42,43] MgO,[42–45] TiO_2,[39,41,46] ZrO_2,[39,41,45,47] HT,[48–50] and HAP.[44,45,51,52] N_2 isotherms and associated surface areas are displayed in **Figure S2**. Changes in the crystalline structure of the materials resulting from the alkaline conditions during catalyst preparation were investigated by XRD (**Figure S3**). CaO and MgO are unstable under such alkaline conditions, which is confirmed by the appearance of additional phases in the diffractograms of the dried Au-loaded catalysts after their preparation. CaO started out as Portlandite ($Ca(OH)_2$, PDF: 01-044-1481) containing a small quantity of lime (CaO, PDF: 01-077-2376) and was fully transformed to Portlandite during preparation of Au/CaO. Similarly, periclase (MgO, PDF: 01-076-9192) was the only phase observed for MgO but a substantial amount of brucite ($Mg(OH)_2$, PDF: 01-080-2856) was formed during the preparation of Au/MgO. Owing to their intrinsic solubility in water and phase changes during catalyst preparation, CaO and MgO are unsuitable supports for aqueous-phase catalytic reactions. In contrast, γ-Al_2O_3, TiO_2, ZrO_2, HT, and HAP supports were stable during catalyst preparation and were deemed suitable for further screening. No diffraction lines belonging to metallic gold were observed, suggesting the absence of large gold crystallites for all prepared catalysts.

Crude HMF-acetal was used for the initial screening of supported Au catalysts. **Figure 1** shows HMF-acetal conversion, the product distribution, and the PDO recovery for each of the tested catalysts. The reactions were conducted at 373 K for 5 h with 10 wt% HMF-acetal solutions containing 2 mol. eq. Na_2CO_3 to HMF-acetal and supported Au catalysts. Crude HMF-acetal contains approximately 12 wt% free PDO as a consequence of the excess PDO used during its preparation. Therefore, PDO recovery in this figure was based on the sum of free PDO derived from the impurity of HMF-acetal synthesis and PDO obtained from the acetal moieties of the reactant and the reaction products by acid hydrolysis during HPLC analysis. All acetal compounds in the reaction mixture were quantitatively detected in their deprotected form by using an acidic eluent during HPLC analysis. All catalysts yielded FFCA as the major product. Despite high PDO recovery (> 85%), Au/HT was less active than the other catalysts, leading to moderate reactant conversion (~ 65%) and FFCA selectivity (~ 45%). Au/TiO_2, Au/ZrO_2, Au/Al_2O_3, and Au/HAP could completely convert 10 wt% HMF-acetal within 5 hours. Surface areas of the bare supports (**Figure S2**) range from 11.4 $m^2 g^{-1}$ to 150 $m^2 g^{-1}$ in the order HAP ≈ ZrO_2 < HT ≈ TiO_2 < Al_2O_3. These data indicate that variations in the catalytic performance are likely not related to changes in the surface area of the support as Au/HAP (S_{BET} = 11.4 $m^2 g^{-1}$) and Au/Al_2O_3 (S_{BET} = 150 $m^2 g^{-1}$) work equally well. Au/Al_2O_3 and Au/HAP provided high FFCA yields and PDO recoveries of approximately 85% and 70%, respectively, which are superior to those for Au/TiO_2, and Au/ZrO_2. The lower FFCA yields and PDO recoveries of Au/TiO_2 and Au/ZrO_2 catalysts can be ascribed to Lewis acid-catalyzed acetal deprotection and degradation phenomena as earlier observed for the Au/CeO_2 system.[20,53] To understand these results more clearly, FT-IR measurements using CO as a probe molecule were conducted for three amphoteric oxides, namely TiO_2, Al_2O_3 and HAP, to evaluate acid strength of Lewis acid sites (**Figure S4**). The blue-shift of the stretching vibration mode of CO adsorbed on acid sites relative to the vibrational mode of free CO in the gas phase (2143 cm^{-1}) can be used to assess the acid strength.[54–56] The CO stretching frequency appeared at 2168 cm^{-1} for HAP, while it was located at 2187 cm^{-1} for Al_2O_3 and TiO_2. These represents Lewis acid sites of these amphoteric oxides. The peak areas of the spectra normalized by sample weight provide a rough estimation of the acid site densities. Comparing the spectra at a CO pressure in the 21-24 Pa range, the CO IR band for TiO_2 (**Figure S4(c), h**) is much larger than the one for HAP (**Figure S5(a), b**) and Al_2O_3 (**Figure S4(b), b**). Thus, a high density of stronger Lewis acid sites negatively affects the FFCA selectivity and PDO recovery. The large number of relatively strong Lewis acid sites on TiO_2 lead to deprotection of FFCA-acetal. Subsequent oxidative degradation of free PDO by Au nanoparticles resulted in a low PDO recovery (52%) for Au/TiO_2 compared to Au/HAP (72%) and Au/Al_2O_3 (71%). Based on these results and its stability during catalyst preparation and during the oxidation of HMF-acetal with Na_2CO_3 under hot alkaline conditions (**Figure S3**), Au/HAP was chosen as a catalyst for further study (**Figure 1**). The Al_2O_3 support and the fresh Au/Al_2O_3 catalyst comprise γ-Al_2O_3 (PDF: 00-010-0425) and Gibbsite ($Al(OH)_3$, PDF: 00-033-0018). However, used Au/Al_2O_3 catalyst mainly consists of Dawsonite ($Na_2AlCO_3(OH)_2$, PDF: 00-045-1359), resulting from reaction with Na_2CO_3 under hot alkaline conditions. In contrast, no structural changes occurred for the HAP support as neither degradation of the original hydroxyapatite phase nor formation of any new phases was observed after impregnation with Au nanoparticles and after use in catalytic reactions. Selective FFCA formation accompanied by high PDO recovery using HAP as the support can therefore be primarily explained by acetal protection using PDO (**Table S2**).

Aerobic oxidation of nonprotected HMF in water was reported to proceed via the formation of HMFCA and FFCA as shown in **Scheme 1a**.[12–20] In such reactions, the oxidation of

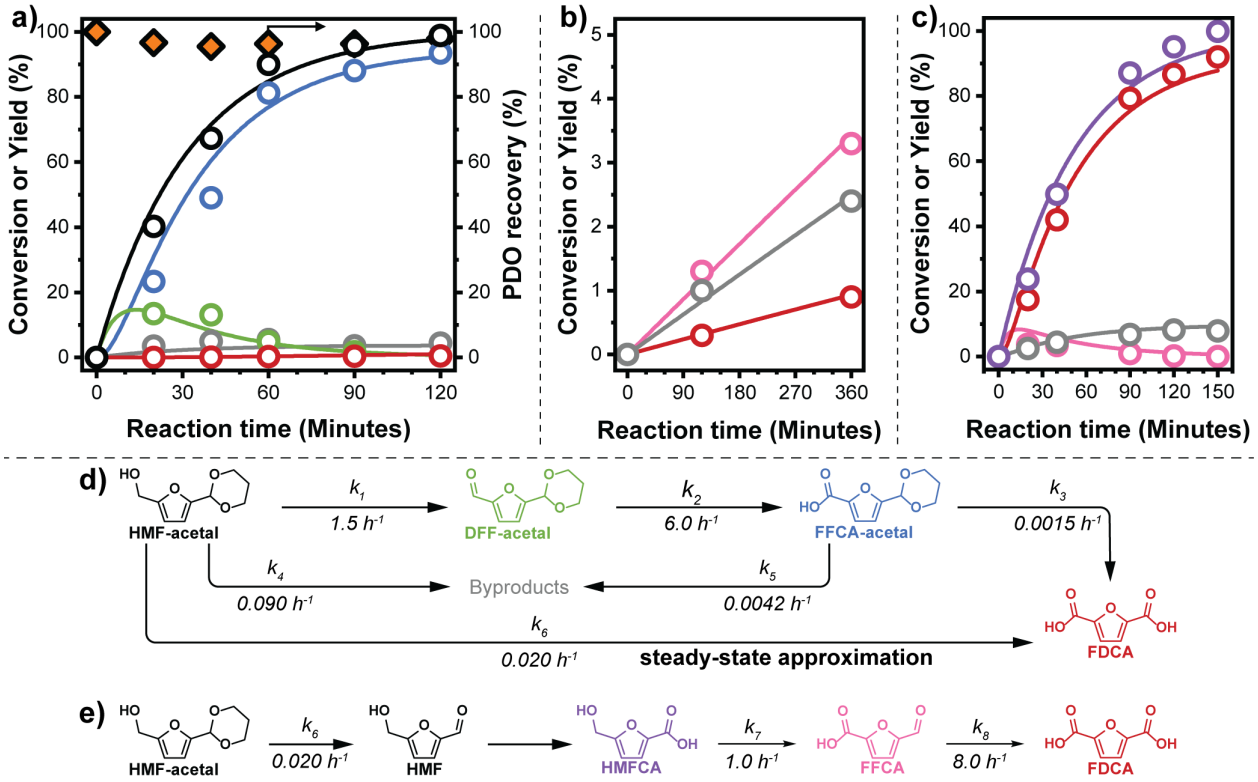

Figure 2. Time courses for (a) FFCA-acetal formation from HMF-acetal, (b) oxidation of FFCA-acetal to FDCA, and (c) oxidation of HMFCA to FDCA with Au/HAP, where substrate concentration in all experiments is 10 wt%. Time course plots were modelled assuming pseudo-first-order reactions using all experimental data points. Open circles in black, blue, green, red, purple, pink, and grey resemble conversion or yield of HMF-acetal, FFCA-acetal, DFF-acetal, FDCA, HMFCA, FFCA, and unidentified byproducts, whereas orange diamonds represent PDO recovery. (d) and (e) represent reaction paths in HMF-acetal oxidation with Au/HAP with reaction rate constants estimated from kinetic traces in (a), (b), and (c). Conditions: HMF-acetal (a), FFCA-acetal (b), or HMFCA (c), 100 mg; catalyst, 100 mg Au/HAP (HMF-acetal/Au = 104 mol/mol); Na_2CO_3, 2 mol. eq. to substrate; H_2O, 1 mL; O_2, 0.5 MPa; 373 K, 750 rpm.

HMFCA to FFCA is considered the rate-determining step and subsequent oxidation of FFCA to FDCA is relatively easy. Consequently, FFCA is usually obtained as a minor fraction in gold-catalyzed HMF oxidation.[18,19,57] In addition, HMF oxidation in concentrated solution leads inevitably to the formation of heavy byproducts, named humins. In contrast, the six-membered ring acetal stabilizes the reactive formyl group against complex side-reactions, even at high concentration (10 wt%), and changes the reaction path, as the hydroxymethyl group in HMF-acetal is converted to the carboxylic acid with retention of the cyclic acetal through DFF-acetal as an intermediate (**Scheme 1b**). Therefore, FDCA can be obtained through the sequential oxidation of HMF-acetal to DFF-acetal and FFCA-acetal. Obtaining FFCA in high yields over HMFCA therefore implies that the oxidation mainly proceeds with retention of the acetal protecting group and most likely yields acetal-protected FFCA as a main product. High PDO recovery strongly suggests the formation of FFCA-acetal to be pronounced under the reaction conditions, because free PDO formed by deprotection should be involved in oxidative degradation and additional byproduct formation (**Table S2**).

We reported the oxidation of the acetal moiety as the rate-determining step in the HMF-acetal oxidation, in which hemiacetal formation from the cyclic acetal catalyzed by the Lewis acid sites of the inorganic support, contributes substantially to efficient FDCA formation (**Scheme S1**).[20] Au/HAP produced very little FDCA, in line with our hypothesis that the weakly Lewis acidic and basic HAP support is ineffective for hemiacetal formation, despite the intrinsic ability of Au nanoparticles towards oxidation of aldehydes and primary alcohols.[20] Consequently, Au/HAP successfully stops HMF-acetal oxidation at FFCA-acetal. The difference between PDO recovery (70%) and FFCA yield (85%) for Au/HAP is probably due to oxidative degradation of free PDO contained in the substrate, which is caused by a long residence time. Complete degradation of free PDO contained in HMF-acetal (12 wt% in 100 mg) corresponds to 25% of the total PDO (free + PDO-protected HMF-acetal), which means that a part of free PDO is involved in oxidative degradation.

A kinetic study was performed to assess the optimal reaction time, the reaction paths and the corresponding reaction rate constants for 1 wt% Au/HAP catalyst (**Figure 2a)**. Here, purified HMF-acetal (purity: 95%) was used to more closely monitor PDO degradation, stemming only from PDO liberated through acetal deprotection, and to limit any influence of oxidized PDO products on the reaction. The kinetic traces in these figures were modeled assuming pseudo-first order kinetics. The oxidation of HMF-acetal was initiated from its hydroxymethyl moiety to produce DFF, which gave the reaction rate constant of k_1 = 1.5 h^{-1}. Subsequent oxidation of DFF to FFCA proceeded faster with a larger reaction rate constant of k_2 = 6.0 h^{-1}. A two-hour reaction afforded the maximum FFCA yield of 94% (95% selectivity) with a PDO recovery of 98% (**Figures 2a** and **2d**). ^{1}H NMR measurements using the reaction mixture at 2 hours and

three standard compounds (FFCA-acetal, DFF-acetal and nonprotected FFCA) verified that FFCA is present only in the acetal form in the reaction mixture, i.e., a signal of the formyl group at 9.5 ppm is absent (**Figure S5**). Therefore, DFF and FFCA detected by HPLC can be regarded as the corresponding acetals as shown in **Figure 2a**. The stability of the FFCA-acetal was confirmed in a kinetic study of FFCA-acetal oxidation using Au/HAP under the same reaction conditions (**Figure 2b**). The kinetic traces indicated that FFCA-acetal oxidation proceeds very slowly with a reaction rate constant of k_3 = 0.0015 h^{-1} (**Figure 2d**), which is negligibly small compared to the rate constants of HMF-acetal (k_1 = 1.5 h^{-1}) and DFF-acetal (k_2 = 6.0 h^{-1}) oxidation. This large difference suggests that deprotection and subsequent oxidation of FFCA-acetal contributes only to a marginal extent to FDCA formation during HMF-acetal oxidation. A small reaction rate constant for byproduct formation from FFCA-acetal in **Figures 2b** and **2d** (k_5 = 0.042 h^{-1}), together with results of additional control experiments in **Table S3** also indicate the high stability of FFCA-acetal towards oxidative and non-oxidative degradation. Therefore, the formation of FDCA and byproduct in **Figure 2a** is related to the stability of HMF-acetal, because deprotected HMF can be involved in FDCA formation as illustrated in **Scheme 1a** or side-reactions. In HMF-acetal oxidation in **Figure 2a**, the yield of undetectable byproduct was increased to approximately 5% in the first hour and remained almost constant for the next one hour. The rate for undetectable byproduct formation from HMF-acetal was estimated at k_4 = 0.090 h^{-1}.

To clarify the formation of FDCA and byproducts, we examined the stability of HMF-acetal with several control experiments (**Table S4**). HMF-acetal was perfectly stable in the absence of Au/HAP under the reaction conditions (**Table S4, entry 3**). HAP support itself slightly promoted the degradation of HMF-acetal (**Table S4, entry 2**). This minor degradation may be due to deprotection of the acetal moiety by the Lewis acid sites present on HAP support, forming HMF with a reactive formyl group. In HMF-acetal oxidation, such deprotected HMF formed in the reaction mixture participates in side-reactions for humin formation as well as its aerobic oxidation catalyzed by Au nanoparticles to produce HMFCA, FFCA, and FDCA (**Figure 2e**). It should be noted that neither deprotected HMF nor any intermediates obtained upon its oxidation (HMFCA and non-protected FFCA) were observed. This implies that such intermediates are much more rapidly oxidized under the applied reaction conditions than HMF-acetal is deprotected. The rate constant of FDCA formation from HMF-acetal was found to be k_6 = 0.020 h^{-1}, assuming this is a single step (**Figure 2d**). This assumption for k_6 can be validated from control experiments using HMFCA as a reactant. Aerobic oxidation of nonprotected HMF in situ formed by deprotection of HMF-acetal produces FDCA via HMFCA and FFCA as shown in **Figure 2e**. HMF oxidation using a concentrated solution (10 wt%) and Au/CeO_2 resulted in small amounts of FDCA (< 30%) and heavy byproduct formation (> 70% yield) as reported in our previous work.[20] In the current reaction system, deprotection of HMF-acetal is a minor path, resulting in a very low concentration of deprotected HMF in the reaction mixture. Consequently, stepwise oxidation of deprotected HMF to FDCA is much more favorable than byproduct formation. When HMFCA was used as a substrate under the same reaction conditions (**Figure 2c**), kinetic traces revealed selective oxidation of HMFCA to FDCA

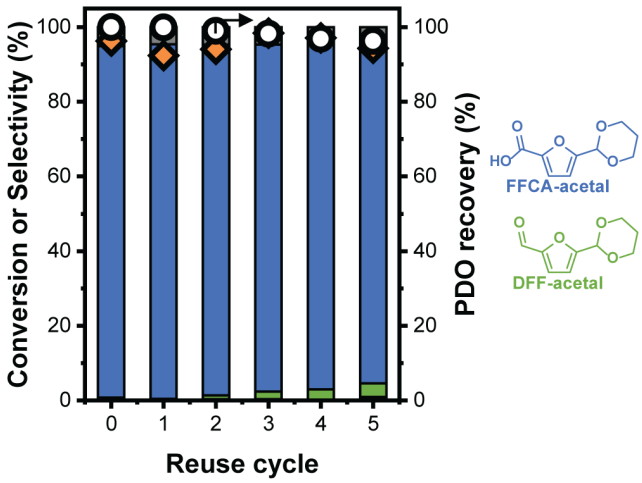

Figure 3. Reuse experiment of Au/HAP for HMF-acetal oxidation to FFCA-acetal. Blue, green, and grey bars show the yield of FFCA-acetal, DFF-acetal, and unidentified byproducts, respectively, while orange diamonds and white circles represent PDO recovery and HMF-acetal conversion. Conditions: HMF-acetal, 100 mg; catalyst, 100 mg Au/HAP (HMF-acetal/Au = 104 mol/mol); Na_2CO_3, 2 mol. eq. to HMF-acetal; H_2O, 1 mL; O_2, 0.5 MPa; 373 K, 2 h, 750 rpm.

with large reaction rate constants for HMFCA oxidation to FFCA (k_7 = 1.0 h^{-1}) and FFCA oxidation to FDCA (k_8 = 8.0 h^{-1}) compared to k_6 (= 0.020 h^{-1}). These oxidation rates and the rate for HMF-acetal deprotection thus differ by two orders of magnitude, implying that HMF formed by HMF-acetal deprotection is oxidized almost as soon as it is formed. As such, the FDCA formation from HMF-acetal can be summarized as a single step with rate k_6 = 0.020 h^{-1} (**Figure 2e**).

A reuse experiment was conducted for Au/HAP using purified HMF-acetal (**Figure 3**). The catalyst was recovered by centrifugation, washed with water, and dried at 353 K after every cycle. While the fresh catalyst produced FFCA-acetal as the main product in 94% yield (95% selectivity) and DFF-acetal in <1% yield, the activity slowly dropped during the remaining 4 cycles, yielding 88% FFCA-acetal (91% selectivity), accompanied by a 4% yield (4% selectivity) of DFF-acetal. The PDO recovery remained stable at an average of 96%. The Au/HAP catalyst was additionally examined for deactivation during the early stages of the reaction (Figure S6). Reactions were performed using similar conditions as above for a reaction time of 20 min, which limits the conversion to below 40%. The fresh catalyst yielded 20% FFCA-acetal at 37% conversion accompanied by a DFF-acetal yield of 15% yield with less than 1% of byproducts, while the PDO recovery was 95%. The catalyst was then reused twice after being washed and dried overnight for every cycle. No significant changes in conversion, product yield, and PDO recovery were observed, even during the initial stage of the reaction, supporting the claim that Au/HAP can be reused for at least 5 cycles without significant losses in performance.

To address the reason for the small but observable loss in performance, the catalyst was examined by XRD and HAADF-STEM. **Figure S3** shows XRD patterns of the fresh and used Au/HAP catalysts. The support remains unaffected by the reaction experiments, but a broad diffraction assignable to the

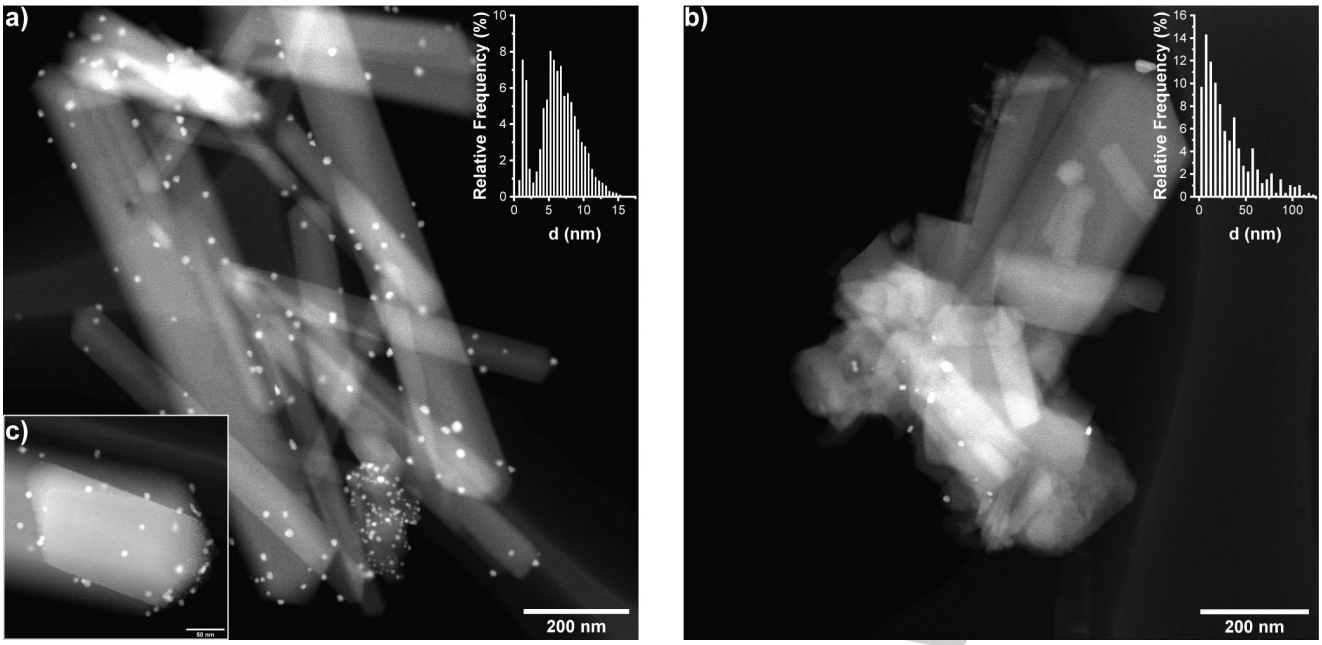

Figure 4. HAADF-STEM images of (a) fresh, and (b) used HAP after 6 consecutive uses. Insert c) shows presence of ~1 nm sized particles. Histograms in both figures indicate particle size distribution.

(111) plane of metallic Au appeared in all used catalysts. As this feature is absent in the fresh catalyst and for the HAP support, we can infer that the gold particles grow during the catalytic oxidation reaction. Such particle growth was also observed for the other Au catalysts (**Figure S3**). It was found that, during the first run, Au nanoparticles agglomerate mostly during the first 20 minutes. The average Au particle size at this stage, determined by XRD, increased to 15 nm. Prolonging the reaction to 5 hours leads to an average particle size of 17 nm. After 5 consecutive reuses, the particle size was 25 nm. HAADF-STEM analysis (**Figures 4** and **S7**) was conducted to investigate fresh and used Au/HAP in more detail. Fresh Au/HAP (**Figure 4a**) presents a bimodal particle size distribution: small and well-dispersed Au particles ranging from 0.5 nm to 2.5 nm with an average diameter of 1.6 nm are predominant on the perimeter of the HAP support material, while larger Au particles with diameters from 2.5 nm up to 15 nm with an average size of 7.2 nm were found scattered over the support surface.

HAADF-STEM analysis of the used material (**Figure 4b**) displays a broad particle size distribution. The Au nanoparticles in the Au/HAP reused 5 times range from 0.7 nm up to 125 nm in diameter. The average of 21 nm is close to the value determined by XRD. It can be seen that the small particles present on the edges of the material are replaced by larger particles and even clusters of gold particles (**Figures 4b** and **S7**). The exact mechanism for this kind of particle growth is not well understood, but it is likely that the alkaline environment can cause the aggregation of gold species into larger particles. To exclude the role of soluble Au species in the catalytic reaction, a hot-filtration test was carried out. For this purpose, the Au/HAP catalyst was removed after reaching a conversion of 70% after 30 min (**Table S5**). The yield of oxidation products did not increase during the next 1.5 h in the absence of Au/HAP, confirming the heterogeneous nature of the reaction.

The second step of the current approach, deprotection of the acetal, was first studied by using a concentrated solution (10 wt%) of as-synthesized FFCA-acetal in water containing 2 molar equivalents Na_2CO_3. Addition of Na_2CO_3 is necessary to facilitate dissolution of the FFCA-acetal through neutralization of the carboxylic acid. Deprotection was facilitated by lowering the pH to 1 with 37% HCl and stirring this mixture at 338 K for 4 hours. ^{1}H NMR was used to determine the progress of acetal deprotection (**Figure S1**), which showed that the yield of free FFCA was 99% (**Scheme 2**). Separation of the FFCA from the aqueous phase was accomplished by extraction with EtOAc. A mere 3% PDO was entrained in the organic phase after extraction (**Figure S1**), while the majority of PDO (94%) formed by deprotection of FFCA-acetal remained in the water phase. This means that the deprotection step of the intermediate FFCA-acetal in the overall process can be carried out with high efficiency with respect to FFCA formation and PDO recovery (**Scheme 2**). This procedure was applied to a reaction mixture containing FFCA-acetal produced in the two-hour reaction of HMF-acetal oxidation (**Figure 2**), from which FFCA-acetal was obtained in 94% yield with 98% PDO recovery. In this case, addition of Na_2CO_3 was not required as the FFCA-acetal was already present in its neutralized and water-soluble state. Here, deprotection of FFCA-acetal afforded free FFCA in 98% yield and PDO in 95% recovery from the reaction mixture (**Scheme 2**),

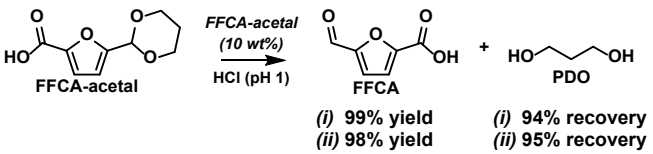

Scheme 2. Deprotection efficiency of 10 wt% FFCA-acetal (obtained from commercial sources or from oxidation of HMF-acetal). FFCA-acetal was produced from: *(i)* commercial reagents; *(ii)* oxidation of HMF-acetal.

Table 1. Oxidation of FFCA to FDCA.[a]

#	Catalyst	FFCA (wt%)	Na_2CO_3 (mol. eq.)	X_{FFCA} (%)	Y_{FDCA} (%)	Y_{HMFCA} (%)	Y_{other} (%)
1	Au/HAP	15	1.5	100	96	0	4
2		20	1.5	100	96	0	4
3		25	1.5	98	82	0	16
4		20	1.25	100	96	0	14
5	Au/CeO_2	20	1.5	100	71	0	29
6	Au/HT	20	1.5	92	32	23	37

[a] Conditions: FFCA, 150-250 mg; Au/HAP, 150-250 mg (weight ratio of FFCA/catalyst = 1, FFCA/Au = 137 mol/mol); Na_2CO_3 (1.25 or 1.5 mol. eq. to FFCA); H_2O, 0.75-0.85 mL; O_2, 0.5 MPa; 413 K, 5 h, 750 rpm.

giving overall FFCA yield in 92% and total PDO recovery in 96% after the second step.

The flexibility of the stepwise approach is further demonstrated in the final step, i.e. the oxidation of FFCA to FDCA using the same Au/HAP catalyst (**Table 1**). The higher stability of FFCA compared to HMF or even HMF-acetal allows more concentrated solutions of FFCA to be used at higher reaction temperatures, and with less Na_2CO_3. Oxidation of FFCA to FDCA was examined at 413 K for 5 hours using non-protected FFCA solutions (15−25 wt%), Au/HAP catalyst, and Na_2CO_3 (1.5 molar equivalents to FFCA). Note that 0.5 equivalents of Na_2CO_3 are inevitably consumed by the initial neutralization reaction of the carboxylic acid group of FFCA. The reactions were facile, affording FDCA in 96% yield at 100% conversion using 15 wt% and 20 wt% FFCA solutions (**entries 1 and 2**). FDCA can be selectively recovered as a white precipitate from the reaction mixture by controlling the pH of the solution. A further increase in FFCA concentration to 25 wt% led to byproduct formation and a low FFCA yield (82%) at an FFCA conversion of 98% (**entry 3**). The reduction of Na_2CO_3 from 1.5 to 1.25 equivalents in a 20 wt% FFCA solution provided FDCA in a moderate yield of 86% at full conversion (**entry 4**). These results suggest that an excess amount of Na_2CO_3 (≥ 1.5 equivalent) is necessary for efficient FDCA formation from free FFCA under the reaction conditions, whereas one equivalent Na_2CO_3 is theoretically sufficient to neutralize both the original carboxylic acid of the FFCA substrate and the newly formed carboxylic acid of the resulting FDCA. Au/CeO_2 and Au/HT were examined as reference catalysts in FFCA oxidation using 20 wt% solutions (**entries 5** and **6**), where Au/CeO_2 was synthesized by a deposition-precipitation method in reference to our previous paper.[20,53] Au/CeO_2 or Au/HT gave lower FDCA yields and higher byproduct yields than Au/HAP (**entries 2**, **5**, and **6**). Byproducts mainly derived from humin-type insolubles were observed as brown precipitates in the reaction mixtures. Au/HT produced significant amounts of HMFCA (23%) and humin-type byproducts (37%). HMFCA formation from FFCA under oxidative reaction conditions means that the Cannizzaro reaction is facilitated by the highly alkaline environment, which produces equal amounts of FDCA and HMFCA through disproportionation of two FFCA molecules. The absence of any HMFCA with Au/HAP or Au/CeO_2 indicates that FFCA oxidation is predominant for FDCA formation in these reactions. In terms of FDCA yield, Au/HAP can be regarded as an active and selective catalyst for FFCA oxidation in concentrated solutions.

The Au/HAP catalyst was similarly tested for any signs of early-stage deactivation for FFCA oxidation to FDCA using the optimized conditions (20 wt% FFCA, 1.5 mol eq. Na_2CO_3, 0.5 MPa O_2. 413 K, 1 h), which resulted in a conversion of ~50%. The results summarized in **Figure S8** of the Supporting Information do not indicate any loss of activity during the early stages of the reaction. The first use afforded FDCA in a 47% yield at 49% FFCA conversion. No changes in activity and byproduct formation were obtained after two consecutive reuses, meaning that Au/HAP is a durable catalyst in aerobic oxidation of nonprotected FFCA using concentrated solutions (20 wt%).

Scheme 3 summarizes representative results of the stepwise approach. The overall FDCA yield was 88%, accompanied by a PDO recovery of 96%. The PDO recovery reported in this work is a substantial improvement compared to the 80% PDO recovery reported for the Au/CeO_2-catalyzed one-pot reaction system.[20] The one-pot reaction system requires an energy-intensive purification method to isolate the remaining 80% PDO from the oxidative degradation byproducts such as 3-hydroxypropionic acid and malonic acid. In the stepwise approach, the PDO is separated from the product stream in an intermediate step, in which the reaction solution comprises acetalized FFCA (FFCA-acetal) in an alkaline aqueous solution. Separation of PDO from this reaction solution starts by acidification, which causes hydrolysis of FFCA-acetal to yield FFCA and PDO. FFCA can be extracted by an organic solvent such as ethyl acetate, leaving an acidic solution of only PDO. The absence of oxidative degradation byproducts in the solution greatly simplifies the isolation and purification of PDO. FFCA in the ethyl acetate solution can be extracted using alkaline water, which then serves as the reaction solution for the third oxidation step to produce FDCA.

Overall, FDCA yield in the stepwise approach was slightly lower, but overall FDCA productivity was significantly improved due to the increase in the substrate concentration up to 20 wt% in the third oxidation step. The second and third step are highly efficient, producing their respective products in >95% yield and with >95% selectivity. Higher FFCA and FDCA yields will

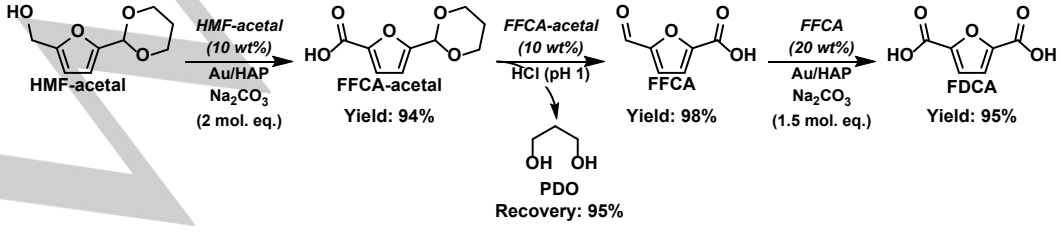

Scheme 3. Outline for the stepwise approach to synthesize FDCA. Left: oxidation of 10 wt% HMF-acetal to FFCA-acetal; Center: deprotection of 10 wt% FFCA-acetal (obtained from oxidation of HMF-acetal); Right: oxidation of 20 wt% FFCA to FDCA.

therefore require further optimization of the first step, in which FFCA-acetal was produced in 94% yield (95% selectivity). After further optimization, we expect that our approach provides a starting point for the development of selective production routes of FFCA and FDCA from concentrated substrate solutions, avoiding formation of large amounts of byproducts and with high recovery of PDO as a protecting agent. High recovery of PDO, high productivity of FFCA and FDCA, and process flexibility in each step are important advantages of the one-pot synthesis of FDCA from HMF and HMF-acetal. Additionally, protection through direct acetalization of HMF and PDO using solid acids such as Amberlyst-15 could be explored to make this initial step more scalable.[58,59] Based on performance data using such methods, a techno-economic analysis would provide insight into the benefit of the protection strategy in terms of productivity of FFCA and FDCA against the drawbacks of adding extra chemical and separation steps.

Conclusion

A protective strategy was developed to maximize FFCA and FDCA yields in the oxidation of HMF. The benefits of the stepwise approach are the ability to use high concentrations of substrates (HMF and FFCA, 10-20 wt%), the ability to obtain the FFCA intermediate (a precursor to other biobased monomers), and high recovery of the protective moiety PDO. Among a series of Au nanoparticle catalysts supported on basic and amphoteric oxides, Au/HAP was the most effective, obtaining intermediate FFCA-acetal in 94% yield after 2 hours at 373 K with a PDO recovery of 98%. The absence of large amounts of FDCA accompanied by a high PDO recovery indicated that the use of a weakly acidic support prevented premature acetal deprotection and consequently halted the further oxidation of FFCA to FDCA as well as the degradation of PDO. The optimum catalyst could be reused for at least 5 runs without drastic loss in performance. Deprotection of FFCA-acetal to obtain FFCA can be effectively achieved by HCl without isolation of the FFCA-acetal from the reaction mixture. FFCA was obtained in 98% yield with a PDO recovery of 95%. The Au/HAP catalyst also proved its utility in the efficient oxidation of a 20 wt% FFCA solution to FDCA, yielding 96% FDCA at full conversion after 5 hours at 413 K. The high PDO recovery benefits FDCA production involving protective chemistry. Current approach to obtain FFCA in high yield opens possibilities to explore its use as a precursor to various other biobased monomers.

Experimental Section

Preparation of supported gold catalysts

Supported gold catalysts were prepared via basic deposition-precipitation using a range of basic or amphoteric oxide supports, i.e. CaO, MgO, TiO_2, ZrO_2, Al_2O_3, HT, and HAP.[19,20,53] Briefly, $HAuCl_4{\cdot}4H_2O$ (350 mg) dissolved in 160 mL deionized water was adjusted to pH 10 by addition of aqueous 0.2M NaOH solution and then mixed with support (2 g) suspended in 50 mL deionized water. After readjustment of the pH to 10, the mixture was stirred at room temperature for 18 hours in contact with air. Solids were collected by centrifugation and repeatedly washed with deionized water until the supernatant tested negative for presence of Cl^- ions by $AgNO_3$ and then dried overnight at 353 K.

Substrate synthesis

HMF-acetal (1,3-propanediol acetal of 5-hydroxymethylfurfural)

There are several papers dealing with acetalization of HMF with various alcohols in a sustainable manner.[58,59] For example, HMF-acetal can be obtained from HMF, PDO, solid acids such as Amberlyst-15 or $CePO_4$, and optionally tetrahydrofuran as solvent. Here, we adopted a typical procedure of well-established organic chemistry to synthesize HMF-acetal with high efficiency and high purity as shown below, in order to remove any influence of impurities on the catalytic studies. Catalytic $In(OTf)_3$ (100 mg; 0.18 mmol; 1.5 mol% to AcOMF) was added to a solution of AcOMF (2.00 g; 11.9 mmol), PDO (3.00 mL; 41.8 mmol) and TMOF (3.00 mL; 27.3 mmol) in DCM (120 mL). The clear and pale-yellow solution was stirred at room temperature overnight and then filtered through a plug of neutral alumina to remove the $In(OTf)_3$ catalyst. DCM was removed by vacuum evaporation and the residual yellowish oil was dissolved in a mixture of EtOH (50 mL) and aqueous Na_2CO_3 solution (10 g Na_2CO_3 in 150 mL deionized water). The clear and slightly yellowish solution was stirred at room temperature for 4 hours to promote hydrolysis of the acetate moiety. EtOH was then removed by vacuum evaporation and the remaining aqueous solution was extracted repeatedly by EtOAc (3 times, ~50 mL in total). The combined organics were dried over $MgSO_4$ and then filtered. EtOAc was removed by vacuum evaporation and the product was received as a yellowish viscous oil in 88%-93% yield and 90% purity on average based on ^{1}H nuclear magnetic resonance (NMR) using DMF as internal standard, accompanied by approximately 12 wt% of free PDO resulting from the excess added in the beginning of the reaction. The isolated product was used as crude HMF-acetal without further purification for the initial screening of supported Au catalysts. The crude HMF-acetal was purified by column chromatography to remove excess PDO (SiO_2 gel, hexane:EtOAc 3:2 by volume. Rf ≈ 0.20) and resulting HMF-acetal with 95% purity was used for further studies. ^{1}H NMR (400 MHz, $CDCl_3$): 6.39 (d, 1H), 6.27 (d, 1H), 5.56 (s, 1H), 4.60 (s, 2H), 4.25 (m, 2H), 3.95 (m, 2H), 2.24 (m, 1H), 1.45 (m, 1H).

FFCA-acetal (1,3-propanediol acetal of 5-formylfuran carboxyl acid)

Amberlyst-15 was added to a mixture of FFCA (1.00 g, 7.14 mmol), PDO (585 µL, 8.16 mmol), and THF (30 mL). The mixture was heated at 333 K for 12 h. The solid catalyst and solvent were removed by filtration and vacuum evaporation, respectively, affording a flaky broken-white solid in 98% yield. The isolated product was used as FFCA-acetal without further purification. ^{1}H NMR (400 MHz, THF-*d8*): 7.17 (d, 1H), 6.58 (d, 1H), 5.64 (s, 1H), 4.10 (m, 2H), 3.92 (m, 2H), 2.00 (m, 1H), 1.45 (m, 1H).

Deprotection procedure of as-synthesized FFCA-acetal

FFCA-acetal (100 mg) was dissolved in 1 mL deionized H_2O, aided by addition of a small quantity of Na_2CO_3, after which the pH was lowered to 1 with 37 wt% HCl. This solution was stirred for 4 hours at 338 K to promote acetal deprotection. The furanics were extracted with EtOAc (4 times, ~2 mL in total) and the combined organics were dried over $MgSO_4$. EtOAc was removed by vacuum evaporation and the product was obtained as an off-white powder in 99% yield. Acetal removal was verified by ^{1}H NMR using THF-*d8* (**Figure S1**).

Characterization

^{1}H NMR spectra were recorded on an JEOL Ltd. ECX 400 NMR spectrometer. Proton chemical shifts are reported in parts per million (ppm) downfield from tetramethylsilane (TMS) using the solvent residual signal as internal standard. HAADF-STEM analysis was performed on a JEOL JEM-ARM200F atomic resolution electron microscope at an acceleration voltage of 200 kV. Finely-ground samples were dispersed into ethanol prior to deposition on carbon-coated copper grids. Particle

size distributions were measured using ImageJ. Roughly 60 images averaging 50 particles per image were analyzed for statistical relevance. Powder X-ray diffraction (XRD) patterns were obtained from a Rigaku Ultima IV diffractometer using Cu Kα radiation (λ = 0.15418 nm, tube voltage of 40 kV, 20 mA current) with a scanning speed of 2° min^{-1} in the range of 10° ≤ 2θ ≤ 70°. Crystal phases were identified using the Rigaku PDXL-2 data analysis software package and the PDF-2 crystallographic database (version 2019). Acid strength analysis was performed with FT-IR (IRSpirit, Shimadzu, DTGS detector), using CO as probe molecule. A total of 64 spectra (spectral resolution: 4 cm^{-1}) were taken per data point and averaged. Finely powdered samples were pressed into self-supporting wafers (20 mm diameter, ~50 mg) and then introduced into an IR cell connected to a closed-glass circulation system. Prior to CO adsorption, the samples were evacuated at 473 K for 2 hours to remove physisorbed water and then cooled down to 100 K with liquid nitrogen. CO was then introduced in controlled amounts until saturation was observed. Each spectrum was measured after adsorbed CO and gaseous CO were in equilibrium. The spectrum taken at 100 K before CO adsorption was used as the baseline for obtaining difference spectra of CO-adsorbed samples. Elemental analysis of reaction liquors was obtained by ICP using a Shimazu ICPE-9000. Liquid samples (1-2 mL) were acidified with 0.4 mL aqua regia (1:3 concentrated HNO_3:HCl by volume) and then diluted to 10.00 mL. Catalyst samples (10-20 mg) were digested in 0.2 mL aqua regia (1:3 concentrated HNO_3:HCl by volume) and then diluted to 50.00 mL Quantification was based on linear response factors using gold standard solutions of known concentration.

Catalytic activity measurements

All catalytic experiments were conducted in Teflon-lined stainless-steel autoclaves (TAIATSU Techno, 10 mL internal volume) which were charged with substrate (100 mg), catalyst (0 or 100 mg), Na_2CO_3 (2 mol. equivalents with respect to the substrate) and water (1 mL). The autoclaves were repeatedly purged with O_2 or N_2 prior to pressurizing to 0.5 MPa and heated in a pre-heated oil bath to 338 K or 373 K for a specified reaction time (0 - 6 hours), while stirred at 750 rpm. After reaction, the contents of the autoclave were diluted with deionized water to dissolve solid products, and the catalyst was recovered by centrifugation. The reaction liquors were analyzed by high-performance liquid chromatography (HPLC; Nexera X2, Shimadzu) equipped with refractive index (RID-10A) and UV-Vis (SPD-20A) detectors. Analytes were separated on an Aminex-HPX-87H column (308 K) using 5 mM H_2SO_4 as mobile phase with a flow rate of 0.5 mL min^{-1} and furanics were quantified by the UV-Vis detector. PDO was quantified separately using a Shodex Sugar SH1011 column (308 K) and refractive index detector, using water as a mobile phase at 0.5 mL min^{-1}. Deprotection of the acetals (HMF-acetal, DFF-acetal and FFCA-acetal) proceeds quantitatively during the HPLC analysis under the influence of 5 mM H_2SO_4 and water used as eluents.[20] Product quantification was based on molar response factors determined by five-point calibration lines obtained by injecting solutions of commercial compounds with known concentrations. PDO recovery is defined as analytical recovery: the amount of PDO present after conducting the oxidation reaction as determined by HPLC is compared to the amount that should theoretically be present.

FFCA and FDCA can be recovered from the reaction mixture by neutralizing the alkaline solution, which causes them to precipitate. Similarly, the propanediol can be separated from the aqueous layer after FFCA extraction in the second step by the addition of methanol, causing the sodium salts to precipitate out. Propanediol can then be recovered through evaporation of water and methanol from the salt-free mixture.

Acknowledgements

This work was supported by JST-MIRAI program (Grant number JPMJMI19E3), Japan. A part of this work was also supported by JSPS Grant-in-Aid for Transformative Research Areas (A) "Hyper-Ordered Structures Science (20H05879)", JSPS Fostering Joint International Research (B) (18KK0135), and the Cooperative Research Program of Institute for Catalysis, Hokkaido University (20A1002).

Keywords: biomass • FDCA • heterogeneous catalysis • HMF • protection strategy

[1] M. Garside, "Global plastic production from 1950 to 2018 (in million metric tons)*," can be found under https://www.statista.com/statistics/282732/global-production-of-plastics-since-1950/, **2018**.

[2] A. D. Moreno, P. Alvira, D. Ibarra, E. Tomás-pejó, *Production of Platform Chemicals from Sustainable Resources*, Springer Singapore, Singapore, **2017**.

[3] P. Gallezot, *Chem. Soc. Rev.* **2012**, *41*, 1538–1558.

[4] R.-J. van Putten, J. C. van der Waal, E. de Jong, C. B. Rasrendra, H. J. Heeres, J. G. de Vries, *Chem. Rev.* **2013**, *113*, 1499–1597.

[5] A. F. Sousa, C. Vilela, A. C. Fonseca, M. Matos, C. S. R. Freire, G. J. M. Gruter, J. F. J. Coelho, A. J. D. Silvestre, *Polym. Chem.* **2015**, *6*, 5961–5983.

[6] J. He, S. P. Burt, M. Ball, D. Zhao, I. Hermans, J. A. Dumesic, G. W. Huber, *ACS Catal.* **2018**, *8*, 1427–1439.

[7] B. Xiao, M. Zheng, X. Li, J. Pang, R. Sun, H. Wang, X. Pang, A. Wang, X. Wang, T. Zhang, *Green Chem.* **2016**, *18*, 2175–2184.

[8] A. B. Dros, O. Larue, A. Reimond, F. De Campo, M. Pera-Titus, *Green Chem.* **2015**, *17*, 4760–4772.

[9] S. Nishimura, K. Ebitani, *J. Japan Pet. Inst.* **2017**, *60*, 72–84.

[10] S. H. Pyo, J. H. Park, V. Srebny, R. Hatti-Kaul, *Green Chem.* **2020**, *22*, 4450–4455.

[11] J. J. Pacheco, M. E. Davis, *Proc. Natl. Acad. Sci. U. S. A.* **2014**, *111*, 8363–8367.

[12] E. Hayashi, T. Komanoya, K. Kamata, M. Hara, *ChemSusChem* **2017**, *10*, 654–658.

[13] F. Neaţu, R. S. Marin, M. Florea, N. Petrea, O. D. Pavel, V. I. Pârvulescu, *Appl. Catal. B Environ.* **2016**, *180*, 751–757.

[14] B. Siyo, M. Schneider, J. Radnik, M. M. Pohl, P. Langer, N. Steinfeldt, *Appl. Catal. A Gen.* **2014**, *478*, 107–116.

[15] Y. Wang, K. Yu, D. Lei, W. Si, Y. Feng, L. L. Lou, S. Liu, *ACS Sustain. Chem. Eng.* **2016**, *4*, 4752–4761.

[16] G. Yi, S. P. Teong, Y. Zhang, *Green Chem.* **2016**, *18*, 979–983.

[17] T. Gao, Y. Yin, W. Fang, Q. Cao, *Mol. Catal.* **2018**, *450*, 55–64.

[18] N. K. Gupta, S. Nishimura, A. Takagaki, K. Ebitani, *Green Chem.* **2011**, *13*, 824–827.

[19] O. Casanova, S. Iborra, A. Corma, *ChemSusChem* **2009**, *2*, 1138–1144.

[20] M. Kim, Y. Su, A. Fukuoka, E. J. M. Hensen, K. Nakajima, *Angew. Chem. Int. Ed.* **2018**, *57*, 8235–8239.

[21] G. Guidotti, M. Soccio, N. Lotti, M. Gazzano, V. Siracusa, A. Munari, *Polymers (Basel).* **2018**, *10*, 785.

[22] M. Vannini, P. Marchese, A. Celli, C. Lorenzetti, *Green Chem.* **2015**, *17*, 4162–4166.

[23] Y. Long, R. Zhang, J. Huang, J. Wang, Y. Jiang, G. H. Hu, J. Yang, J. Zhu, *ACS Sustain. Chem. Eng.* **2017**, *5*, 9244–9253.

[24] H. Hu, R. Zhang, J. Wang, W. Bin Ying, J. Zhu, *ACS Sustain. Chem.*

Eng. **2018**, *6*, 7488–7498.
[25] M. Soccio, M. Costa, N. Lotti, M. Gazzano, V. Siracusa, E. Salatelli, P. Manaresi, A. Munari, *Eur. Polym. J.* **2016**, *81*, 397–412.
[26] H. Hu, R. Zhang, L. Shi, W. Bin Ying, J. Wang, J. Zhu, *Ind. Eng. Chem. Res.* **2018**, *57*, 11020–11030.
[27] H. Xie, L. Wu, B. G. Li, P. Dubois, *Biomacromolecules* **2019**, *20*, 353–364.
[28] L. Genovese, N. Lotti, V. Siracusa, A. Munari, *Materials (Basel).* **2017**, *10*, 1028.
[29] S. K. Burgess, O. Karvan, J. R. Johnson, R. M. Kriegel, W. J. Koros, *Polymer* **2014**, *55*, 4748–4756.
[30] S. K. Burgess, R. M. Kriegel, W. J. Koros, *Macromolecules* **2015**, *48*, 2184–2193.
[31] S. K. Burgess, D. S. Mikkilineni, D. B. Yu, D. J. Kim, C. R. Mubarak, R. M. Kriegel, W. J. Koros, *Polymer* **2014**, *55*, 6870–6882.
[32] J. G. Rosenboom, D. K. Hohl, P. Fleckenstein, G. Storti, M. Morbidelli, *Nat. Commun.* **2018**, *9*, 1–7.
[33] A. H. Motagamwala, W. Won, C. Sener, D. M. Alonso, C. T. Maravelias, J. A. Dumesic, *Sci. Adv.* **2018**, *4*, DOI 10.1126/SCIADV.AAP9722.
[34] M. Talebi Amiri, G. R. Dick, Y. M. Questell-Santiago, J. S. Luterbacher, *Nat. Protoc.* **2019**, *14*, 921–954.
[35] X. Luo, Y. Li, N. K. Gupta, B. Sels, J. Ralph, L. Shuai, *Angew. Chem. Int. Ed.* **2020**, *59*, 11704–11716.
[36] L. Shuai, M. T. Amiri, Y. M. Questell-Santiago, F. Héroguel, Y. Li, H. Kim, R. Meilan, C. Chapple, J. Ralph, J. S. Luterbacher, *Science* **2016**, *354*, 329–333.
[37] United States Environmental Protection Agency, "Basics of green chemistry," **2015**.
[38] J. P. Klein, *Compounds and Methods for Producing Nylon 6*, **2018**, US009982094B2.
[39] C. Lahousse, A. Aboulayt, F. Maugé, J. Bachelier, J. C. Lavalley, *J. Mol. Catal.* **1993**, *84*, 283–297.
[40] A. Takagaki, J. C. Jung, S. Hayashi, *RSC Adv.* **2014**, *4*, 43785–43791.
[41] M. V Zakharova, F. Kleitz, F.-G. Fontaine, *Dalt. Trans.* **2017**, *46*, 3864.
[42] M. Calatayud, A. M. Ruppert, B. M. Weckhuysen, *Chem. - A Eur. J.* **2009**, *15*, 10864–10870.
[43] A. M. Ruppert, J. D. Meeldijk, B. W. M. Kuipers, B. H. Erné, B. M. Weckhuysen, *Chem. - A Eur. J.* **2008**, *14*, 2016–2024.
[44] S. Hanspal, Z. D. Young, H. Shou, R. J. Davis, *ACS Catal.* **2015**, *5*, 1737–1746.
[45] I. M. Hill, S. Hanspal, Z. D. Young, R. J. Davis, *J. Phys. Chem. C* **2015**, *119*, 9186–9197.
[46] K. Nakajima, R. Noma, M. Kitano, M. Hara, *J. Phys. Chem. C* **2013**, *117*, 16028–16033.
[47] T. Komanoya, K. Nakajima, M. Kitano, M. Hara, *J. Phys. Chem. C* **2015**, *119*, 26540–26546.
[48] D. P. Debecker, E. M. Gaigneaux, G. Busca, *Chem. - A Eur. J.* **2009**, *15*, 3920–3935.
[49] D. W. J. Leung, C. Chen, J. C. Buffet, D. O'Hare, *Dalt. Trans.* **2020**, *49*, 9306–9311.
[50] F. Prinetto, G. Ghiotti, R. Durand, D. Tichit, *J. Phys. Chem. B* **2000**, *104*, 11117–11126.
[51] S. Diallo-Garcia, M. Ben Osman, J. M. Krafft, S. Casale, C. Thomas, J. Kubo, G. Costentin, *J. Phys. Chem. C* **2014**, *118*, 12744–12757.
[52] V. Bolis, C. Busco, G. Martra, L. Bertinetti, Y. Sakhno, P. Ugliengo, F. Chiatti, M. Corno, N. Roveri, *Philos. Trans. R. Soc. A Math. Phys. Eng. Sci.* **2012**, *370*, 1313–1336.
[53] M. Kim, Y. Su, T. Aoshima, A. Fukuoka, E. J. M. Hensen, K. Nakajima, *ACS Catal.* **2019**, *9*, 4277–4285.
[54] A. A. Tsyganenko, E. Escalona Platero, C. Otero Areán, E. Garrone, A. Zecchina, *Catal. Letters* **1999**, *61*, 187–192.
[55] D. A. Boyd, F. M. Hess, G. B. Hess, *Surf. Sci.* **2002**, *519*, 125–138.
[56] M. Klein, U. Neugebauer, A. Gheisari, A. Malassa, T. M. A. Jazzazi, F. Froehlich, M. Westerhausen, M. Schmitt, J. Popp, *J. Phys. Chem. A* **2014**, *118*, 5381–5390.
[57] Y. Y. Gorbanev, S. K. Klitgaard, J. M. Woodley, C. H. Christensen, A. Riisager, *ChemSusChem* **2009**, *2*, 672–675.
[58] H. Chang, G. W. Huber, J. A. Dumesic, *ChemSusChem* **2020**, *13*, 5213–5219.
[59] S. Kanai, I. Nagahara, Y. Kita, K. Kamata, M. Hara, *Chem. Sci.* **2017**, *8*, 3146–3153.

Entry for the Table of Contents

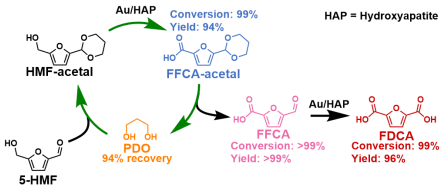

Representation of the stepwise approach for oxidation of HMF-acetal to FDCA, with efficient recycling of the 1,3-propanediol protective agent.

WILEY-VCH